IEEE Transactions on Power Electronics, 2015, Vol. 30, Iss. 6, pp. 3242-3251

State-Space Modelling of a Class E^2 Converter for Inductive Links

Patrick C. K. Luk, *Senior Member, IEEE*, Samer Aldhaher, Weizhong Fei,
James F. Whidborne, *Senior Member, IEEE*

***Abstract*—This paper presents a state-space based analysis of a Class E^2 converter for wireless power systems based on a two-coil inductive link. The Class E^2 converter consists of a 200 kHz Class E inverter as the primary coil driver and a voltage-driven Class E synchronous rectifier at the secondary coil of the inductive link. A piecewise linear 7th order state-space model is used to calculate several parameters and values to achieve optimum switching operation of the Class E inverter and the Class E rectifier. Simulation results are presented to compare the accuracy of the state-space modelling approach with the established analytical approach. For validation of the state-space analysis, an investigation of the influence of variation of coil alignment and load for a 20 W Class E^2 converter prototype system is performed by means of a novel compensation method that maintains optimum switching conditions irrespective of variations. Experimental results are presented to confirm the accuracy of the state-space modelling approach over a wide range of operational conditions and the utility of the compensation method.**

***Index Terms*—Inductive power transmission, DC-DC Resonant converters, Rectifiers.**

I. Introduction

The Class E inverter has been one of the preferred design topologies to be used as the primary coil driver in recent contactless and wireless power transfer (WPT) applications due to its design simplicity, high power delivering capability, sinusoidal output current and efficient operation [1]–[7]. The Class E inverter consists of a single power MOSFET, hence simplifying the MOSFET gate driving circuitry, overall board layout and thermal considerations. On the other hand, Class E rectifiers provide an efficient AC/DC rectification for high frequency AC voltages [3], [8]–[10]. They operate at resonance and have a near sinusoidal input current which makes them suitable for WPT applications. A Class E rectifier was initially used in a WPT system operating at 800 kHz in [3] where an efficiency of 94 % had been achieved. Extensive analysis has been carried out in for Class E inverters in [11]–[13] and for Class E rectifiers in [3], [8]–[10] and the references therein.

Class E inverters and rectifiers can be combined together to form Class E^2 DC/DC resonant converters. These converters can be used to build high frequency, powerful and efficient DC/DC converters. Extensive research has also been carried out on Class E^2 DC/DC converters over the past three decades [14]–[29].

A Class E^2 converter was initially proposed in [14] for inductive links which had a switching frequency of 200 kHz and delivered 100 W to a constant 100 Ω load at an efficiency of 85.1 %. It consisted of a finite DC-feed Class E inverter and a current-driven Class E voltage-switching rectifier. We continue on the work of [14], [20] by presenting a Class E^2 converter that has a more compact form for medium power applications that operate up to 20 W as specified in the 'Qi' wireless power standard [30], [31]. Compactness is achieved by reducing the component count of the Class E^2 converter used in [14] as a result of the dual use of the inductance of the primary coil to eliminate the resonant inductance of the Class E inverter. Moreover, voltage-driven Class E rectifier with a lower component count is used instead of the current-driven Class E rectifier. A MOSFET is employed to replace the diode of the Class E rectifier to provide an improved performance and efficiency of the overall configuration. Consequently, a novel self-starting MOSFET driving circuitry is developed and to be presented here.

The main aim of this paper is to extend the numerical design approach based on state-space modelling of Class E switching circuits that has been used in [2], [3], [14], [19] to provide an improved analysis of the Class E^2 converter, and to use it to calculate certain parameters and values such as the phase difference between the switching of the switches of the Class E inverter and the Class E rectifier, and the maximum current in the coils of the inductive link. Analytical and simulation results will be presented to show the improved accuracy of the state-space modelling approach over the previous work in analysing Class E^2 converters which has been based on analytical approach. The analytical approach assumed that the Class E inverter section of the converter is operating at high Q factor and that the Class E rectifier section could be represented by an equivalent impedance. It is noted that these analytical models have been validated by experimental results over only limited load ranges and operating conditions. However, in such applications such as WPT, it is highly desirable to have design models that provide accurate performance prediction over a wider load range and variations in coil misalignments.

In order to further validate the state-space method experimentally, an investigation of the influence of variations of coil alignment and load for a 20 W Class E^2 converter prototype system is performed by means of a novel compensation method that maintains optimal operating conditions irrespective of the variations.

This paper is organised as follows. Section II presents the Class E^2 converter. Analysis is carried out based on a 7th order piece-wise linear state-space representation. Section III provides a design example and addresses the effect of coil misalignment and load variation. A comparison is provided between the results obtained from the analysis presented in

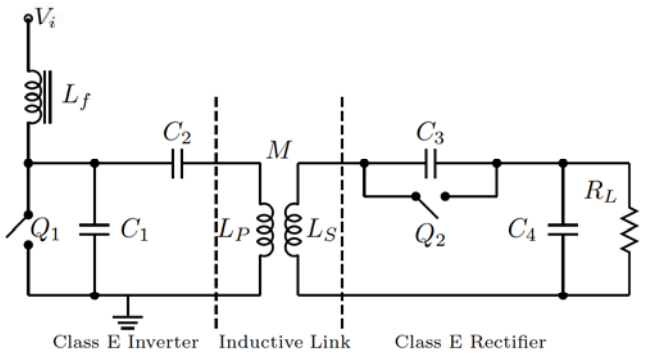

Fig. 1. Circuit of the Class E inverter, inductive link and the Class E rectifier

this paper with the analytical approach. Section IV describes the experimental setup of a Class E^2 converter for an inductive link system and discusses the obtained experimental results. Section V gives the conclusions and suggests further work.

II. Modelling and Analysis

The Class E^2 converter under study consists of a Class E zero-voltage switching (ZVS) and zero-derivative voltage switching (ZDS) inverter with an infinite DC-feed inductance [11], an inductive link consisting of a primary and secondary coils separated by a certain air gap and a voltage-driven Class E ZVS rectifier presented in [3], [32]. Fig. 1 shows the complete circuit of the converter. The inverter and rectifier switches are designated by Q_1 and Q_2 respectively, L_f is the DC-feed inductance of the inverter, L_P and L_S represent the inductances of the primary and secondary coils respectively and M is mutual inductance between them. Resistor R_L represents the load. The ZDS of the Class E inverter means that the first derivative of the voltage across switch Q_1 is zero at the moment it is switched ON, which intern results in zero-current switching. The switches are driven at the same switching frequency ω, but at different duty cycles which will be discussed in the following sections.

A. State-space representation

The Class E^2 converter in Fig. 1 can be represented by the equivalent circuit shown in Fig. 2. Resistors r_P and r_S are included to represent the equivalent series resistance (ESR) of the primary and secondary coils respectively. The analysis will be based on the following two assumptions:

- Switches Q_1 and Q_2 have zero switching times, infinite OFF resistances and ON resistances r_{Q_1} and r_{Q_2} respectively.
- The shunt capacitors C_1 and C_2 absorb the output capacitance of switches Q_1 and Q_2 respectively.

The equivalent circuit can be analysed by the following general state-space representation

$$\dot{X}(\omega t) = AX(\omega t) + BU(\omega t) \tag{1}$$
$$Y(\omega t) = CX(\omega t) + DU(\omega) \tag{2}$$

where X is the state vector and contains the following seven voltage and current states variables

$$X(\omega t) = \begin{bmatrix} v_{C_1}(\omega t) & v_{C_2}(\omega t) & v_{C_3}(\omega t) & v_{C_4}(\omega t) \cdots \\ \cdots & i_{L_f}(\omega t) & i_{L_P}(\omega t) & i_{L_S}(\omega t) \end{bmatrix}^T \tag{3}$$

and U is the input vector equal to a unit step function. Using KVL and KCL, the matrices A, B, C and D are given as

$$A = \begin{bmatrix} \frac{-1}{\omega C_1 r_{Q_1}} & 0 & 0 & \\ 0 & 0 & 0 & \\ 0 & 0 & \frac{-1}{\omega C_3 r_{Q_2}} & \\ 0 & 0 & 0 & \cdots \\ \frac{-1}{\omega L_f} & 0 & 0 & \\ \frac{L_S\alpha}{\omega M^2(1-\alpha)} & \frac{-L_P\alpha}{\omega M^2(1-\alpha)} & \frac{-\alpha}{\omega M(1-\alpha)} & \\ \frac{\alpha}{\omega M(1-\alpha)} & \frac{-\alpha}{\omega M(1-\alpha)} & \frac{-L_P\alpha}{\omega M^2(1-\alpha)} & \end{bmatrix}$$
$$\begin{bmatrix} 0 & \frac{1}{\omega C_1} & \frac{-1}{\omega C_1} & 0 \\ 0 & 0 & \frac{1}{\omega C_2} & 0 \\ 0 & 0 & 0 & \frac{1}{\omega C_3} \\ \cdots \quad 0 & 0 & 0 & \frac{1}{\omega C_4} \\ 0 & 0 & 0 & 0 \\ \frac{-\alpha}{\omega M(1-\alpha)} & 0 & \frac{L_S\alpha r_p}{\omega M^2(1-\alpha)} & \frac{-\alpha r_s}{\omega M(1-\alpha)} \\ \frac{-L_P\alpha}{\omega M^2(1-\alpha)} & 0 & \frac{-\alpha r_p}{\omega M(1-\alpha)} & \frac{L_P\alpha r_s}{\omega M^2(1-\alpha)} \end{bmatrix} \tag{4}$$

$$B = \begin{bmatrix} 0 & 0 & 0 & 0 & \frac{1}{\omega L_f} & 0 & 0 \end{bmatrix}^T \tag{5}$$

$$C = \mathbf{I} \tag{6}$$

$$D = \begin{bmatrix} 0 & 0 & 0 & 0 & 0 & 0 & 0 \end{bmatrix}^T \tag{7}$$

where $\mathbf{I}$ is the 7×7 identity matrix and

$$\alpha = \omega^2(L_P L_S - M^2). \tag{8}$$

B. Switching periods and operating modes

The Class E^2 converter will have four operating modes depending on the state of the switches. The switches are either ON in which they are represented by their ON resistances, or OFF in which they are represented by their OFF resistances.

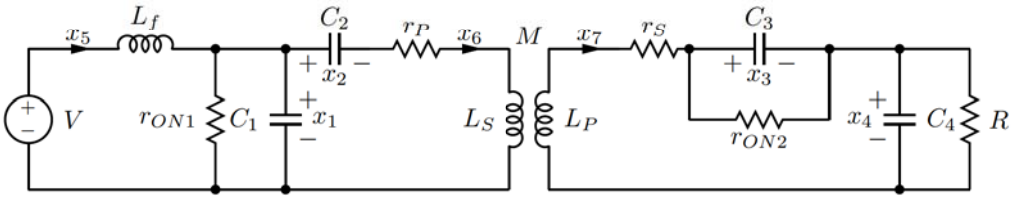

Fig. 2. Equivalent circuit model of the Class E^2 converter.

TABLE I
DEFINITION OF THE OPERATING MODES OF THE CLASS E^2 CONVERTER

Mode	Domain	r_{Q_1}	r_{Q_2}
①	$0 < \omega t \leq 2\pi a$	r_{ON1}	r_{ON2}
②	$0 < \omega t \leq 2\pi(b-a)$	r_{ON1}	∞
③	$0 < \omega t \leq 2\pi(c-a)$	∞	∞
④	$0 < \omega t \leq 2\pi(1-c)$	∞	r_{ON2}

Fig. 3 shows the order of the four different modes in one switching period. It is assumed that the inverter is set to operate at a duty cycle ratio of 0.50. The order of the modes can be initially deduced by inspecting the operation of the circuit. However the duration of each mode is not yet known. The four different operating modes are defined in Table I. The switching period begins in Mode①. In this mode both switches are turned ON and are represented by their ON resistance. At $\omega t = a$, the converter transitions into Mode② and the rectifier's switch is turned OFF. At $\omega t = b$, the converter transitions into Mode③ where the inverter's switch is now turned OFF. At $\omega t = c$, the converters transitions to the final Mode④, where the rectifier's switch is now turned ON and the inverter's is kept OFF. The four modes of operation result in four different A matrices which lead to four different linear state-space representations. The complete model of the converter is now a piecewise linear state-space representation. Fig. 4 shows the voltage waveforms of the switches that are associated with this mode sequence. From Fig. 4, the duty cycle ratio D_1 of switch Q_1 is equal to

$$D_1 = \frac{b}{2\pi} \tag{9}$$

and the duty cycle ratio D_2 of switch Q_2 is equal to

$$D_2 = \frac{2\pi + a - c}{2\pi}. \tag{10}$$

The phase difference ϕ between D_1 and D_2 is equal to

$$\phi = c \tag{11}$$

C. Determining the Initial Conditions of the states

The general solution to Eqs. 1 and 2 is given by

$$X(\omega t) = X_n(\omega t) + X_f(\omega t). \tag{12}$$

Function X_n is the natural response matrix, or the zero-input response matrix, and is equal to

$$X_n(\omega t) = e^{A\omega t} X(0) \tag{13}$$

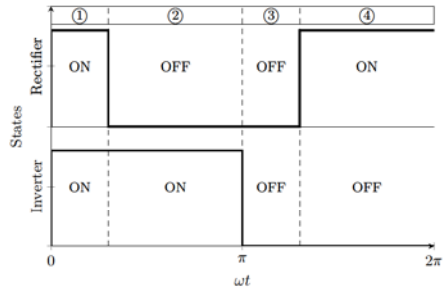

Fig. 3. The possible operating modes of the inverter and rectifier for one switching cycle

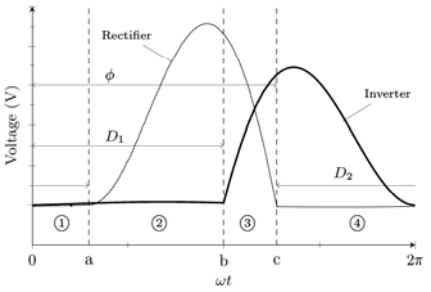

Fig. 4. Voltage waveforms of the inverter MOSFETs Q_1 and the rectifier MOSFET Q_2

where e is the matrix exponential function. $X(0)$ is the initial condition matrix. Function X_f is the forced response matrix, or the zero-state response matrix, and is equal to

$$\begin{aligned} X_f(\omega t) &= \int_0^{\tau} e^{A(\omega t - \tau)} B U(\tau) d\tau \\ &= A^{-1}\left(e^{A\omega t} - \mathbf{I}\right) B. \end{aligned} \tag{14}$$

The initial condition matrix $X(0)$ can be determined from the voltages' and currents' continuity conditions as the converter transitions from one mode to the next as follows

$$X_{①}(0) = X_{④}(2\pi(1-c)) \tag{15}$$
$$X_{②}(0) = X_{①}(2\pi(a)) \tag{16}$$
$$X_{③}(0) = X_{②}(2\pi(b-a)) \tag{17}$$
$$X_{④}(0) = X_{③}(2\pi(c-b)). \tag{18}$$

By substituting Eqs.16-19 in Eq. 12, the initial conditions of all states in all modes are equal to

$$\begin{bmatrix} X_{①}(0) \\ X_{②}(0) \\ X_{③}(0) \\ X_{④}(0) \end{bmatrix} = \begin{bmatrix} -e^{A_{①}2\pi a} & \mathbf{I} & 0 & 0 \\ 0 & -e^{A_{②}2\pi(b-a)} & \mathbf{I} & 0 \\ 0 & 0 & -e^{A_{③}2\pi(c-b)} & \mathbf{I} \\ \mathbf{I} & 0 & 0 & -e^{A_{④}2\pi(1-c)} \end{bmatrix} \cdot \begin{bmatrix} A_{①}^{-1}(e^{A_{①}2\pi a} - \mathbf{I}) \\ A_{②}^{-1}(e^{A_{②}2\pi(b-a)} - \mathbf{I}) \\ A_{③}^{-1}(e^{A_{③}2\pi(c-b)} - \mathbf{I}) \\ A_{④}^{-1}(e^{A_{④}2\pi(1-c)} - \mathbf{I}) \end{bmatrix} B. \quad (19)$$

D. Solving for optimum switching conditions

The modelling and analysis has now been completed. The next step is to determine the values of the components and switching periods for each modes that will achieve the optimum switching conditions of the Class E^2 converter. From Fig. 4, the inverter's optimum ZVS and ZDS conditions occur in Mode① at $\omega t = 0$. The rectifier's optimum ZVS conditions occur in Mode② at $\omega t = a$ and in Mode④ at $\omega t = c$. These optimum switching conditions can be written as

$$V_{DS1}(0) = 0 \;\rightarrow\; x_{①1}(0) = 0 \quad (20)$$

$$\left.\frac{V_{DS1}(\omega t)}{d\omega t}\right|_{\omega t=0} = 0 \;\rightarrow\; x_{①5}(0) - x_{①6}(0) = 0 \quad (21)$$

$$V_{DS2}(2\pi a) = 0 \;\rightarrow\; x_{②3}(0) = 0 \quad (22)$$

$$V_{DS2}(2\pi c) = 0 \;\rightarrow\; x_{④3}(0) = 0 \quad (23)$$

By using Eqs. 19-23, a computer program can be written to solve numerically for the four different component values or parameters. The design example in the following section will discuss this in further details.

III. Design Case

This section will describe the design procedure of a Class E^2 converter prototype for an inductive link. The converter will operate from a 9 V DC supply and will deliver up to 20 W of power to a nominal 10 Ω load at a 200 kHz switching frequency.

A. Initial design

The design procedure begins with coils of the inductive link. The coils should have a large quality (Q) factor at the switching frequency of the converter for maximum power transfer efficiency. Extensive research has been devoted into developing coils for inductive links, and it is outside the scope of this paper. For this reason, the popular 'Qi' Wireless Power Consortium standard [31] is adopted in determining the primary and secondary coils. Both coils have a maximum DC resistance of 0.1 Ω, an inductance of 24 µH and a maximum Q factor of 230 at 200 kHz [33]. The coils' ESR can be calculated and is equal to 0.137 Ω. With the addition of the connectors' resistance and the DC resistance of the printed circuit board tracks, the total resistance of the coils is approximately 0.180 Ω at 200 kHz. The mutual inductance between the primary and secondary coils can be measured at different separation distances. For a separation distance of 3 mm, the measured mutual inductance is approximately 12 µH which corresponds to a coupling coefficient (k) value of 0.50.

The secondary coil of the inductive link and capacitor C_3 form the resonant part of the Class E rectifier. The value of C_3 that will cause the rectifier to resonate at 200 kHz is equal to

$$C_3 = \frac{1}{\omega^2 L_P} = 26.38\,\text{nF} \quad (24)$$

The output capacitor C_4 should be large enough to maintain a constant DC voltage. A value of 6.6 µF is found to be suitable. The duty cycle D_2 of switch Q_2 and its phase ϕ with respect to D_1 are the first two parameters that will need to be determined from Eqs. 19-23.

The DC-feed inductor L_f of the Class E inverter should be large enough to maintain a constant DC current flow. A choke with a 1 mH inductance is used. The duty cycle D_1 of switch Q_1 is initially set at 0.50. MOSFET IRF540 was used for both switches Q_1 and Q_2. The total resistance of the MOSFETs' drain-to-source channel and the printed circuit board trace is approximately 0.15 Ω. Capacitors C_1 and C_2 are the two remaining values that will need to be determined from Eqs. 19-23.

The values and parameters that need to be determined are now a, c, C_1 and C_2. Eqs. 19-23 were programmed in MATLAB using the Optimization Toolbox and Simulink was then used to measure voltages and currents throughout the converter. The code is included in the Appendix. Table II lists the solutions obtained for D_2, C_1 and C_2. Table II also lists the maximum voltages across the switches $V_{Q_1\text{max}}$ and $V_{Q_2\text{max}}$, the maximum current in the switches $I_{Q_1\text{max}}$ and $I_{Q_2\text{max}}$, the input average DC current I_{In}, the primary coil's peak-to-peak current I_{Lp}, the output voltage across the load V_o and the overall DC-to-DC efficiency η. The solutions and measurements for three coupling coefficient values above and below the nominal value of 0.50 are included to show how the variation in the distance between the coils affects the converter. It can be seen that as the coils are further away from each other, or at loose coupling coefficients, the converter delivers more power to the load but at increased current stresses and reduced efficiencies. Efficiency is reduced due to the increasing currents in the coils which lead to higher ohmic losses. The converter delivers less power to the load as the coils are brought closer to each other or at tighter coupling coefficients. The duty cycle D_2 and phase ϕ remain relatively constant when the coupling coefficient varies. This is because the Class E rectifier's performance is mainly affected by the load [3], [32] which is kept constant at 10 Ω.

Table III lists the solutions and measurements for several load values above and below the nominal load. The distance between the coils is kept constant at a coupling coefficient

TABLE II
CALCULATED PARAMETERS FOR A VARIABLE COUPLING COEFFICIENT AND FIXED LOAD OF $10\,\Omega$

k	f(kHz)	D_1	D_2	ϕ	C_1(nF)	C_2(nF)	$V_{Q_1\max}$(V)	$V_{Q_2\max}$(V)	$I_{Q_1\max}$(A)	$I_{Q_2\max}$(A)	I_{In}(A)	I_{Lp}(A)	V_o(V)	η%
0.35	200	0.500	0.511	229.347	99.656	33.269	31.407	56.133	9.547	4.066	3.333	12.541	14.835	73.37
0.40	200	0.500	0.511	229.489	80.302	35.989	31.530	51.572	7.682	3.746	2.676	10.106	13.607	76.88
0.45	200	0.500	0.511	229.657	66.003	39.663	31.618	47.433	6.287	3.457	2.196	8.288	12.562	79.84
0.50	**200**	**0.500**	**0.511**	**229.864**	**55.230**	**44.773**	**31.683**	**43.736**	**5.223**	**3.202**	**1.820**	**6.905**	**11.571**	81.74
0.55	200	0.500	0.510	230.124	46.972	52.208	31.729	40.447	4.397	2.977	1.538	5.833	10.760	83.64
0.60	200	0.500	0.510	230.464	40.552	63.826	31.759	37.510	3.744	2.780	1.305	4.989	10.010	85.31
0.65	200	0.500	0.509	230.931	35.509	84.251	31.777	34.864	3.219	2.608	1.126	4.314	9.336	86.01

TABLE III
CALCULATED PARAMETERS FOR A VARIABLE LOAD AND A FIXED COUPLING COEFFICIENT OF 0.5

$R(\Omega)$	f(kHz)	D_1	D_2	ϕ	C_1(nF)	C_2(nF)	$V_{Q_1\max}$(V)	$V_{Q_2\max}$(V)	$I_{Q_1\max}$(A)	$I_{Q_2\max}$(A)	I_{In}(A)	I_{Lp}(A)	V_o(V)	η%
5	200	0.500	0.573	217.428	84.266	40.459	31.514	42.683	8.091	4.827	2.822	10.644	9.621	72.89
6	200	0.500	0.558	220.590	75.623	41.297	31.563	43.104	7.249	4.338	2.527	9.544	10.156	75.59
8	200	0.500	0.532	225.742	63.462	43.005	31.632	43.555	6.048	3.657	2.112	7.978	10.992	79.46
10	**200**	**0.500**	**0.511**	**229.864**	**55.230**	**44.773**	**31.683**	**43.736**	**5.223**	**3.202**	**1.820**	**6.905**	**11.571**	81.74
15	200	0.500	0.470	237.587	42.731	49.581	31.784	43.703	3.946	2.526	1.380	5.247	12.623	85.53
20	200	0.500	0.440	243.215	35.561	55.168	31.888	43.395	3.196	2.152	1.125	4.277	13.338	87.85
30	200	0.500	0.395	251.291	27.455	70.145	32.114	42.538	2.326	1.756	0.824	3.158	14.158	90.10
50	200	0.500	0.337	261.584	19.844	144.43	32.580	40.671	1.491	1.430	0.539	2.091	14.964	92.32

of 0.50. The converter delivers more power to higher loads at increased current stress and reduced efficiencies. The output voltage is also reduced. At reduced loads, the converter delivers less power but at higher efficiencies. The duty cycle D_2 and phase ϕ vary accordingly since now the load does change. These variations will have to be considered and may increase the complexity of the driving circuitry for switch Q_2.

It is noted that solutions listed in Tables II and III are not unique, other solutions exist that satisfy the optimum switching conditions. However they are not considered further since they suffer from implementation difficulties and poor efficiencies.

B. Comparison with the analytical approach

It is necessary to compare the proposed state-space approach with the analytical approach [8]–[10], [20], [23]–[26] in terms of accuracy and complexity. In this section, certain solutions will be obtained using the analytical approach to determine the level of agreement to those in Tables II and III.

The analytical approach begins by representing the inductive link with an T-equivalent circuit [34] as shown in Fig. 5a. Next, the Class E rectifier part is replaced with an equivalent inductor L_{EQ} and equivalent resistor R_{EQ} as shown in Fig. 5b. Further details on determining the equivalent inductance and resistance of selected Class E rectifier topology in this paper can be found in [32]. Finally, the components in the output network of the Class E inverter can be represented by an equivalent inductor L_x and equivalent load resistance R_x as shown in Fig. 5c. Setting the duty cycle to D_1 to 0.50, the values of C_1 and C_2 can be determined using the design equations in [2], [35].

Table IV compares between the solutions obtained using the two approaches for two load values of $10\,\Omega$ and $30\,\Omega$. For the $10\,\Omega$ load case, the solutions for C_1, C_2 and D_2 in both approaches are relatively close to each other. However for the $30\,\Omega$ load case, the difference between the solutions of both approaches starts to increase. It can be assumed that the analytical approach is less accurate for the $30\,\Omega$ load case since the Q factor of the inverter is reduced. As a result, the

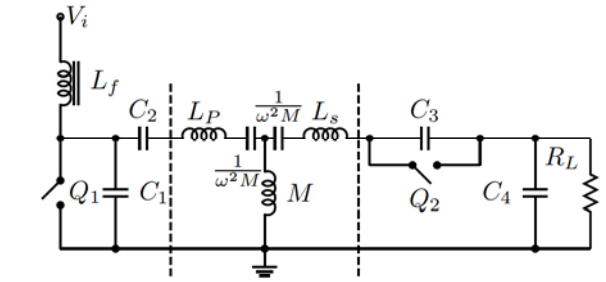

(a) Replacing the inductive link with a T-equivalent circuit

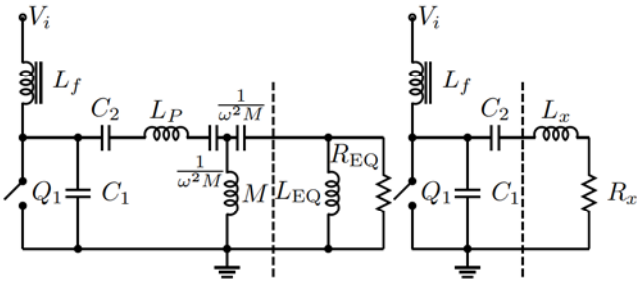

(b) Replacing the Class E rectifier with an equivalent impedance

(c) Replacing the output network of the Class E inverter with an equivalent impedance

Fig. 5. Equivalent circuits of the Class E^2 converter for the analytical approach

current in coils of the inductive link is no longer sinusoidal, therefore the assumptions that the analytical approach is based on are not valid. The phase ϕ and output voltage V_o were not determined in the analytical approach since they involve tedious calculations.

PSPICE simulations were performed using the solutions in Table IV for both approaches. Fig. 6 shows the voltage and current waveforms of Q_1 and Q_2 respectively. A difference can be observed in the waveforms due to mismatch in the solutions. It can be seen from the waveforms that the solutions

TABLE IV
CALCULATED VALUES AND PARAMETERS COMPARING THE ANALYTICAL APPROACH WITH THE PIECEWISE LINEAR STATE-SPACE APPROACH

	$R_L = 10\,\Omega$, $k = 0.50$		$R_L = 30\,\Omega$, $k = 0.50$	
	Analytical	State-space	Analytical	State-space
C_1	58.088 nF	55.230 nF	29.666 nF	27.455 nF
C_2	45.195 nF	44.773 nF	76.667 nF	70.145 nF
D_2	0.515	0.511	0.404	0.395
ϕ	-	229.864°	-	251.291°
R_{EQ}	96.463 Ω	-	41.512 Ω	-
L_{EQ}	19.726 µH	-	15.504 µH	-
R_x	2.693 Ω	-	5.842 Ω	-
L_x	16.738 µH	-	14.825 µH	-
V_o	-	11.571 V	-	14.158 V

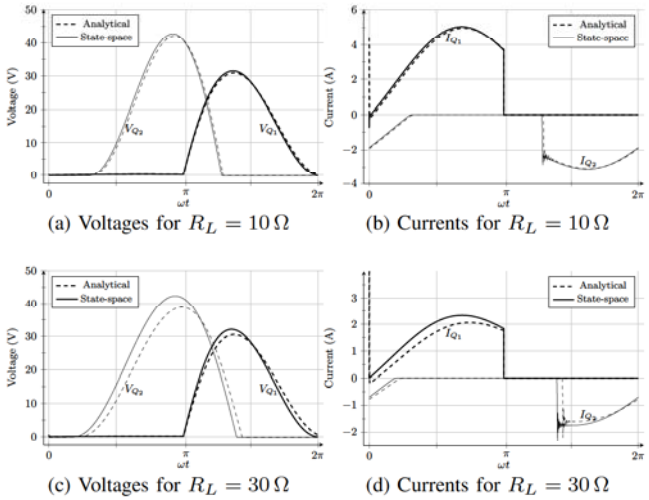

(a) Voltages for $R_L = 10\,\Omega$ (b) Currents for $R_L = 10\,\Omega$

(c) Voltages for $R_L = 30\,\Omega$ (d) Currents for $R_L = 30\,\Omega$

Fig. 6. Simulation results comparing the voltage and current waveforms of Q_1 and Q_2 for the analytical approach and the piecewise linear state-space modelling approach.

obtained using the analytical approach do not completely satisfy the optimum switching conditions of the converter. The voltage across switch Q_1 in Figs. 6a and 6c is not zero when the switch is turned ON. This results in a large current spike to flow through switch Q_1 as can be seen in Figs. 6c and 6d. The analytical approach resulted in a DC output voltage of 11.900 V and 14.093 V for a 10 Ω load and 30 Ω load respectively, whereas the state-space approach resulted in a DC output voltage of 11.571 V and 14.158 V for a 10 Ω load and 30 Ω load respectively.

C. Compensation for load variations and coil misalignments

The Class E^2 converter prototype is to operate at a nominal load of 10 Ω at a coupling coefficient of 0.50. Variations can occur in the load and alignment of the coils while the converter is operating. These variations can cause the Class E inverter to operate at non-optimum switching conditions since Class E inverters can only operate optimally at a constant load value. Tables II and III list the solutions for different load and coupling coefficient values. However it is necessary to alter the values of capacitors C_1 and C_2 to compensate for any variations. Since replacing capacitors may not be practically feasible, it is only reasonable to keep the values of capacitors C_1 and C_2 constant for a specific nominal load and coupling coefficient. Other parameters such as the switching frequency, the duty cycles D_1 and D_2 and phase ϕ can be altered even when the converter is operating [36].

Table V lists the solutions for different values of loads and coupling coefficients when capacitors C_1 and C_2 are kept constant at 53.360 nF and 45.139 nF respectively. Altering the switching frequency will shift the operation of the Class E rectifier part of the converter from resonance. However efficient operation can still be maintained [8].

The solutions in Table V will be verified manually by observing the voltage waveform across switch Q_1. These solutions form the basis for the controllers and algorithms to be implemented to achieve automatic compensation.

IV. EXPERIMENTAL VERIFICATION

A. Implementation and Set-up

A Class E^2 converter was built based on the specifications and the design method presented in the previous sections. The complete circuit is shown in Fig. 7. The Class E inverter part is powered from a 9 V DC supply limited to 2.6 A. The switching signal of MOSFET Q_1 is supplied from a function generator via a MOSFET driver. An electronic load is connected to the output of the Class E rectifier to simulate various loading conditions. The coils of the inductive link are initially kept at a separation distance of 3 mm. A photograph of the experimental setup is shown in Fig. 8.

B. Class E rectifier self-start and driving circuit

Driving MOSFET Q_2 of the rectifier requires additional circuitry to ensure that the switching signal is supplied at the correct instants. Referring to the time instant c in Fig. 4, MOSFET Q_2 switches ON once the voltage across it crosses zero volts. Therefore, the voltage across MOSFET Q_2 can used to trigger the switching signal using a comparator. On the other hand, the voltage across MOSFET Q_2 cannot be relied on as a trigger to turn it OFF. This is because the voltage has a near zero time derivative. Therefore a one-shot timer is used to drive MOSFET Q_2 with a time duration equal to or less than duty cycle D_2. The timer is triggered once the comparator detects a zero crossing in the voltage across MOSFET Q_2.

The Class E rectifier part is an isolated circuit. Power is not available immediately once the converter starts up, therefore the driving circuitry for MOSFET Q_2 will not be functional. However, the rectifier will still be able to start automatically due to the body diode of MOSFET Q_2. Once the output voltage rises to a sufficient level, the driving circuitry will then activate to allow for synchronous operation. A voltage regulator is connected to the output of the rectifier to supply power to the driving circuitry.

C. Results

The Class E^2 converter prototype was operated at a nominal load 10 Ω, a coupling coefficient of 0.50 and a 200 kHz switching frequency. The duty cycle D_1 was set to 0.50 and

TABLE V
CALCULATED PARAMETERS FOR A VARIABLE LOAD AND VARIABLE COUPLING COEFFICIENT

$R(\Omega)$	k	f(kHz)	D_1	D_2	ϕ	$V_{Q_1\max}$(V)	$V_{Q_2\max}$(V)	$I_{Q_1\max}$(A)	$I_{Q_2\max}$(A)	I_{In}(A)	I_{Lp}(A)	V_o(V)	η(%)
5	0.50	187.882	0.590	0.582	221.433	38.166	53.465	10.543	5.854	4.228	12.841	11.768	72.79
6	0.50	190.042	0.571	0.565	223.465	36.597	51.671	8.952	5.063	3.489	11.088	11.917	75.38
8	0.50	194.750	0.535	0.535	226.997	33.915	47.751	6.722	3.954	2.491	8.603	11.932	79.38
10	**0.50**	**200.000**	**0.500**	**0.511**	**229.864**	**31.683**	**43.736**	**5.223**	**3.202**	**1.820**	**6.905**	**11.571**	81.74
12	0.50	205.855	0.465	0.490	232.064	29.750	39.693	4.128	2.640	1.344	5.645	11.025	83.74
14	0.50	212.659	0.426	0.471	233.465	27.894	35.279	3.248	2.169	0.957	4.617	10.120	84.93
10	0.45	187.701	0.543	0.519	228.835	34.499	52.797	6.901	3.704	2.600	8.774	13.726	80.51
10	0.47	192.186	0.526	0.516	229.267	33.373	49.118	6.186	3.504	2.269	7.981	12.876	81.19
10	0.52	206.112	0.480	0.507	230.122	30.536	40.177	4.633	2.990	1.553	6.240	10.729	82.36
10	0.55	217.243	0.444	0.501	229.982	28.689	34.597	3.772	2.632	1.162	5.258	9.312	82.92

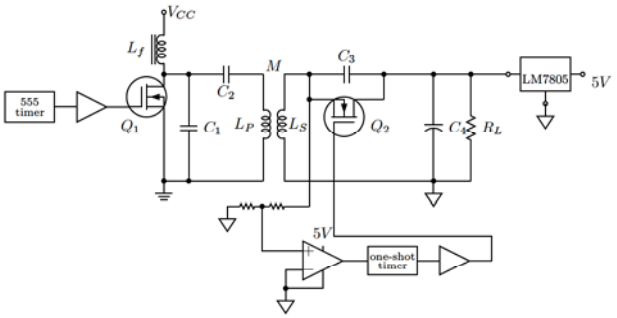

Fig. 7. Circuit of the experimental setup

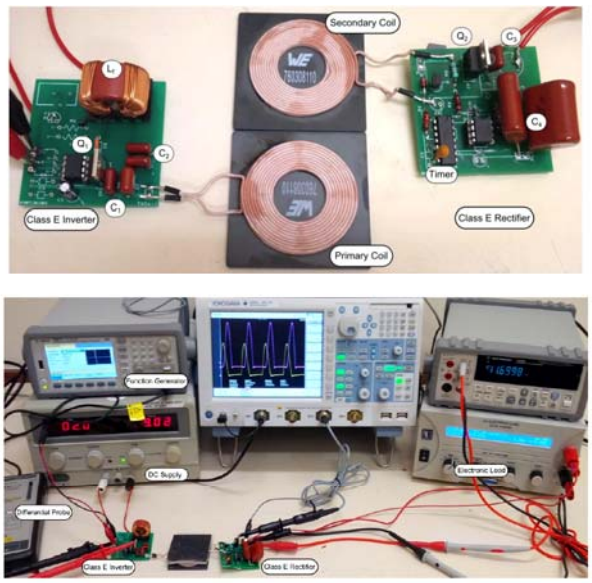

Fig. 8. Photograph of the Class E^2 converter and the experimental setup

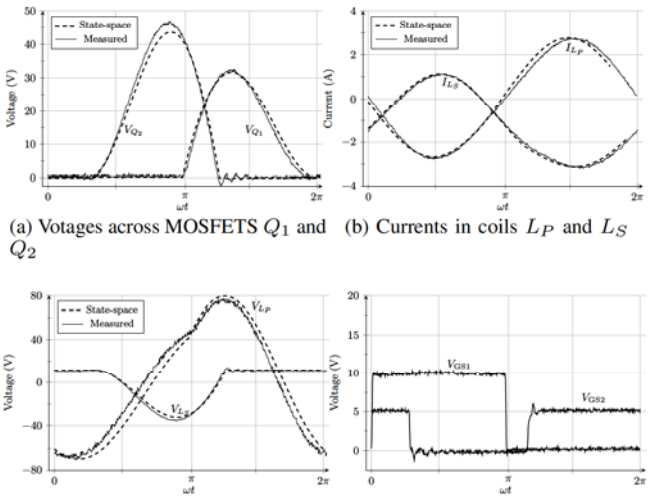

(a) Votages across MOSFETS Q_1 and Q_2 (b) Currents in coils L_P and L_S

(c) Primary coil and secondary coil voltages (d) Switching signals

Fig. 9. Measured waveforms

TABLE VI
CALCULATED PARAMETERS FOR A VARIABLE LOAD AND VARIABLE COUPLING COEFFICIENT

Parameter	Measured	Calculated	Error
V_o(V)	11.53	11.571	-0.35 %
P_o(W)	13.294	13.389	-0.71 %
I_{IN}(A)	1.88	1.820	+3.30 %
η %	78.57	81.74	-3.88 %
$V_{Q_1\max}$(V)	32.6	31.683	+2.89 %
$V_{Q_2\max}$(V)	47.0	44.773	+4.97 %
ϕ°	230	229.864	+0.06 %

the one-shot timer was set to provide a 2.56 µs pulse corresponding to a duty cycle D_2 of 0.51. Fig. 9 shows the observed waveforms of the voltages across MOSFETs Q_1 and Q_2, the currents and voltages of the primary and secondary coils and the switching signals. The waveforms of the piecewise linear state-space model are also plotted for comparison. It can be seen that the observed waveforms are in good agreement with the state-space model. Table VI provides further comparison between several measured and calculated parameters. The errors between the measured and calculated parameters could be attributed to the tolerance of the capacitors' values and parasitic capacitance and inductance in the printed circuit board.

Fig. 10 shows a loss breakdown analysis at nominal operating conditions. Power is mainly lost in the ESR of the inductive link coils, switching and conduction losses in MOSFETs Q_1 and Q_2 and other losses such as that of MOSFET drivers, the ESR of the capacitors and the timing and control circuitry of the rectifier. It can be seen that a significant amount of power is lost the ESR of the inductive link coils, whereas the power lost in the inverter and rectifier is low. Therefore, the overall efficiency can be improved by using coils with lower ESR.

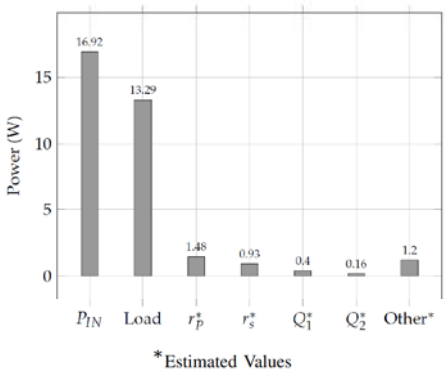

Fig. 10. Power distributions

D. Load Variation

The performance of the Class E^2 converter was investigated for variations in load and coil misalignment as discussed in the previous section. The load was varied from $8\,\Omega$ to $15\,\Omega$ and the coupling coefficient from 0.45 to 0.55. The duty cycles and switching frequencies were varied according to Table V. Fig. 11 shows the measured output voltage, input power and efficiency for both load and coupling coefficient ranges. It can be seen that the measured parameters agree with the calculations in Table V. The overall efficiency is reduced at higher loads and loose coupling coefficients, whereas lower loads and tighter coupling coefficients result in a higher overall efficiencies. The output voltage and output power are largest at loose coupling coefficients and higher loads and decrease as the coupling coefficient increases and the load decreases. The agreement between the measured parameters with the calculations in Table V confirm that the Class E^2 converter can adapt to variations in load and distance in inductive links that may occur during operation. This is due to the result that the Class E inverter part of the converter can be tuned to achieve its optimum switching conditions by adjusting its duty cycle and switching frequency.

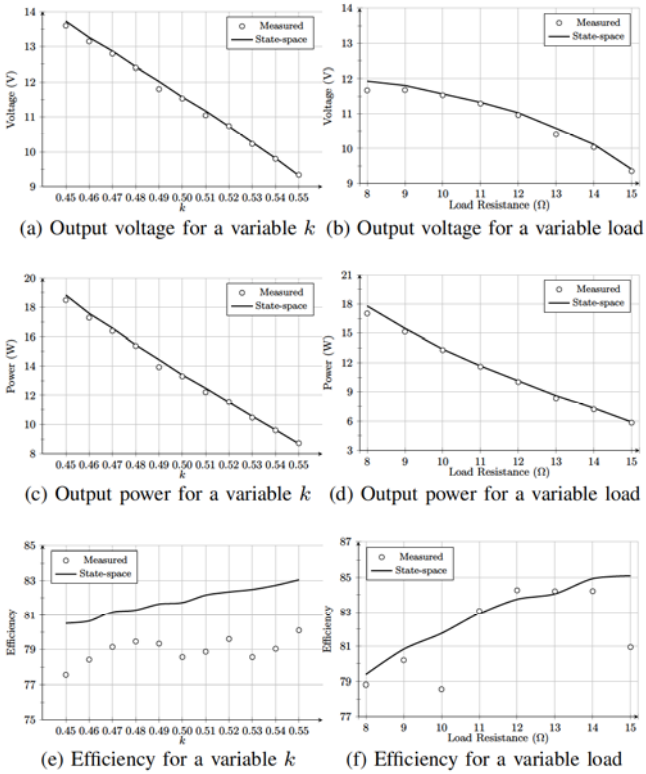

(a) Output voltage for a variable k (b) Output voltage for a variable load

(c) Output power for a variable k (d) Output power for a variable load

(e) Efficiency for a variable k (f) Efficiency for a variable load

Fig. 11. Variation in coupling coefficient and load

V. Conclusions

This paper presents a Class E^2 converter for inductive link which consists of a Class E ZVS and ZDS inverter and a Class E ZVS rectifier. A 7th order piecewise linear state-space model has been used to model converter and the inductive link including the ON resistance of the switches and the ESR of coils. The state-space model is used to calculate the values of the converter's components and parameters for optimum switching conditions. A compensation method is used to adapt for variations in the load and the distance between the coils by adjusting the switching frequency and the duty cycle of the switches.

The accuracy of the state-space model is compared to that of an analytical model. PSPICE simulations show that calculations based on the state-space model satisfy the optimum switching conditions of the converter, whereas calculations derived from the analytical modelling approach do not completely satisfy the optimum switching conditions. Experimental results prove the accuracy of the state-space modelling approach and verify the utility of the compensation method for variations in load level and distance between the coupled coils of the inductive link.

Since the compensation method was implemented manually in the current work, future work may include the development of controllers and algorithms to achieve automatic compensation.

References

[1] S. Aldhaher, P. K. Luk, and J. F. Whidborne, "Tuning Class E inverters applied in inductive links using saturable reactors," *Power Electronics, IEEE Transactions on*, vol. 29, no. 6, pp. 2969–2978, Jun. 2014.

[2] S. Aldhaher, P. C. K. Luk, and J. F. Whidborne, "Wireless power transfer using Class E inverter with saturable DC-feed inductor," in *Proc. IEEE Energy Convers. Congr. Expo.*, Sep. 2013, pp. 1902–1909.

[3] ——, "High input voltage high frequency Class E rectifiers for inductive links," *IEEE Trans. Power Electron...*, to be published.

[4] R. J. Calder, S. H. Lee, and R. D. Lorenz, "Efficient, MHz frequency, resonant converter for sub-meter (30 cm) distance wireless power transfer," in *Proc. IEEE Energy Convers. Congr. Expo.*, 2013, pp. 1917–1924.

[5] M. Pinuela, D. C. Yates, S. Lucyszyn, and P. D. Mitcheson, "Maximizing DC-to-load efficiency for inductive power transfer," *IEEE Trans. Power Electron.*, vol. 28, no. 5, pp. 2437–2447, May 2013.

[6] L. Chen, S. Liu, Y. C. Zhou, and T. J. Cui, "An optimizable circuit structure for high-efficiency wireless power transfer," *IEEE Trans. Ind. Electron.*, vol. 60, no. 1, pp. 339–349, Jan. 2013.

[7] E. M. Thomas, J. D. Heebl, C. Pfeiffer, and A. Grbic, "A power link study of wireless non-radiative power transfer systems using resonant shielded loops," *IEEE Trans. Circuits Syst. I, Reg. Papers*, vol. 59, no. 9, pp. 2125–2136, Sep. 2012.

[8] S. Birca-Galateanu and J.-L. Cocquerelle, "Class E half-wave low dv/dt rectifier operating in a range of frequencies around resonance," *IEEE Trans. Circuits Syst. I, Fundam. Theory Appl.*, vol. 42, no. 2, pp. 83–94, Feb. 1995.

[9] S. Birca-Galateanu and A. Ivascu, "Class E low dv/dt and low di/dt rectifiers: energy transfer, comparison, compact relationships," *IEEE Trans. Circuits Syst. I, Fundam. Theory Appl*, vol. 48, no. 9, pp. 1065–1074, Sep. 2001.
[10] M. K. Kazimierczuk and J. J. Jozwik, "Class-E zero-voltage-switching and zero-current-switching rectifiers," *IEEE Trans. Circuits Syst.*, vol. 37, no. 3, pp. 436–444, Mar. 1990.
[11] M. K. Kazimierczuk and D. Czarkowski, *Resonant Power Converters*, 2nd ed. New Jersey, USA: John Wiley & Sons, 2011.
[12] A. Grebennikov and N. O. Sokal, *Switchedmode RF Power Amplifiers*. Oxford, UK: Newnes, 2007.
[13] M. Kazimierczuk, "Exact analysis of Class E tuned power amplifier with only one inductor and one capacitor in load network," *IEEE Journal of Solid-State Circuits*, vol. 18, no. 2, pp. 214–221, Apr 1983.
[14] T. Nagashima, K. Inoue, X. Wei, E. Bou, E. Alarcon, and H. Sekiya, "Inductively coupled wireless power transfer with class-e2 dc-dc converter," in *Circuit Theory and Design (ECCTD), 2013 European Conference on*, Sept 2013, pp. 1–4.
[15] J. Rivas, O. Leitermann, Y. Han, and D. Perreault, "A very high frequency DC-DC converter based on a Class Φ_2 resonant inverter," *IEEE Trans. Power Electron.*, vol. 26, no. 10, pp. 2980–2992, Oct. 2011.
[16] S. Jalbrzykowski, A. Bogdan, and T. Citko, "A dual full-bridge resonant Class E bidirectional DC/DC converter," *IEEE Trans. Ind. Electron*, vol. 58, no. 9, pp. 3879–3883, Aug. 2011.
[17] R. C. N. Pilawa-Podgurski, A. D. Sagneri, J. M. Rivas, D. I. Anderson, and D. J. Perreault, "Very-high-frequency resonant boost converters," *IEEE Trans. Power Electron.*, vol. 24, no. 6, pp. 1654 – 1665, Jun. 2009.
[18] H. Hase, H. Sekiya, J. Lu, and T. Yahagi, "Resonant DC/DC converter with Class E oscillator," *IEEE Trans. Circuits Syst. I, Reg. Papers*, vol. 53, no. 9, pp. 2025–2035, Sep. 2006.
[19] H. Sekiya, J. Lu, and T. Yahagi, "Design of generalized class e2 dc/dc converter," *International Journal of Circuit Theory and Applications*, vol. 31, no. 3, pp. 229–248, 2003. [Online]. Available: http://dx.doi.org/10.1002/cta.229
[20] I. Boonyaroonate and S. Mori, "Analysis and design of Class E isolated DC/DC converter using Class E low dv/dt PWM synchronous rectifier," *IEEE Trans. Power Electron.*, vol. 16, no. 4, pp. 514–521, Jun. 2001.
[21] Y.-F. Liu and P. Sen, "New Class E DC/DC converter topologies with constant switching frequency," *Industry Applications, IEEE Transactions on*, vol. 32, no. 4, pp. 961–969, Jul. 1996.
[22] W. Gu and K. Harada, "A circuit model for the Class E resonant DC/DC converter regulated at a fixed switching frequency," *IEEE Trans. Power Electron.*, vol. 7, no. 1, pp. 99–110, Aug 1992.
[23] J. J. Jozwik and M. K. Kazimierczuk, "Analysis and design of Class E^2 DC/DC converter," *IEEE Trans. Ind. Electron*, vol. 37, no. 2, pp. 173–183, Aug. 1990.
[24] M. K. Kazimierczuk and X. Bui, "Class E DC/DC converters with an inductive impedance inverter," *IEEE Trans. Power Electron.*, vol. 4, no. 1, pp. 124–135, Jan. 1989.
[25] ——, "Class E DC/DC converters with a capacitive impedance inverter," *IEEE Trans. Ind. Electron*, vol. 36, no. 3, pp. 425–433, 1989.
[26] M. K. Kazimierczuk and J. Jozwik, "Resonant DC/DC converter with Class E inverter and Class E rectifier," *IEEE Trans. Ind. Electron*, vol. 36, no. 4, pp. 468–478, Nov. 1989.
[27] ——, "DC/DC converter with Class E zero-voltage-switching inverter and class E zero-current-switching rectifier," *IEEE Trans. Circuits Syst.*, vol. 36, no. 11, pp. 1485–1488, Nov. 1989.
[28] R. Redl, B. Molnar, and N. Sokal, "Class E resonant regulated DC/DC power converters: Analysis of operations, and experimental results at 1.5 MHz," *IEEE Trans. Power Electron.*, vol. PE-1, no. 2, pp. 111–120, Apr. 1986.
[29] ——, "Small-signal dynamic analysis of regulated Class E DC/DC converters," *IEEE Trans. Power Electron.*, vol. PE-1, no. 2, pp. 121–128, Apr. 1986.
[30] S. Hui, "Planar wireless charging technology for portable electronic products and qi," *IEEE Proc.*, vol. 101, no. 6, pp. 1290–1301, June 2013.
[31] [Online]. Available: http://www.wirelesspowerconsortium.com.
[32] A. Ivascu, M. K. Kazimierczuk, and S. Birca-Galateanu, "Class E resonant low dv/dt rectifier," *IEEE Trans. Circuits Syst. I, Fundam. Theory Appl*, vol. 39, no. 8, pp. 604–613, Aug. 1992.
[33] Würth Elektronik, WE-WPCC Wireless Power Charging Coil 760308110 datasheet.
[34] C. Alexander and M. Sadiku, *Fundamentals of Electric Circuits*, 3rd ed. McGraw-Hill, 2007.
[35] M. K. Kazimierczuk and K. Puczko, "Exact analysis of Class E tuned power amplifier at any Q and switch duty cycle," *IEEE Trans. Circuits Syst. I, Reg. Papers*, vol. 34, no. 2, pp. 149–159, Feb. 1987.
[36] H. Sekiya, H. Koizumi, S. Mori, I. Sasase, J. Lu, and T. Yahagi, "FM/PWM control scheme in Class DE inverter," *IEEE Trans. Circuits and Systems I: Regular Papers*, vol. 51, no. 7, pp. 1250–1260, Jul. 2004.

Patrick Chi-Kwong Luk (M'92-SM'08) was born in Hong Kong. He received the High Diploma with merits (BSc) in electrical engineering from Hong Kong Polytechnic University (PolyU), Hong Kong, in 1983, the M.Phil. degree in electrical engineering from Sheffield University, U.K., in 1989, and the Ph.D. degree in electrical engineering from the University of South Wales in 1992.

He started his career in industry as Engineer Trainee between 1981-83 at GEC (H.K.) and then after graduation as Applications Engineer at Polytek Engineering Co. (H.K.). In 1986, he worked as Senior Researcher in the Industrial Centre, PolyU. Since 1988, he had held academic positions at the University of South Wales, Robert Gordon University, Aberdeen, U.K., and University of Hertfordshire, U.K. He joined Cranfield University, U.K., in 2002, where he is a Chair Professor in Electrical Engineering and Head of the Electric Power and Drives Group in the School of Engineering. He sits in several IEEE Committees on Electrical Machines and is the Chairman of the IEEE UKRI Young Professionals. He is also an Associate Editor for IEEE Transactions on Power Electronics, IEEE Transactions on Smart Grids, and IET Renewable Power Generation. He has over 140 publications and co-holder of several patents in power electronics, motor drives, and control. His main current research interests include electrical drives, renewable energy systems, and high-frequency power electronics.

Currently, he holds Visiting Professorships at Blaise Pascal University in France, and Shanghai Jiao Tong University in China.

Samer Aldhaher received the B.Sc. degree in electrical engineering from the University of Jordan, Amman, Jordan in 2010. He is currently working towards the Ph.D. degree at Cranfield University, Bedford, UK.

His current research interests include the design of high frequency DC/AC inverters, wireless power transfer applications based on resonant inductive links and switched-mode circuits.

Weizhong Fei (M'12) was born in Zhejiang, China. He received the B. Eng. and M. Eng. degrees from Zhejiang University, Hangzhou, China, in 2004 and 2006, respectively, and the Ph. D. degree from Cranfield University, Shrivenham, U.K., in 2010, all in electrical engineering. s From 2011 to 2012, he was a Research Associate at the University of Sheffield, Sheffield, U.K. Since 2012, he has been with the School of Engineering, Cranfield University, where he is currently a Lecturer in Clean Energy Technology. His current research interests include design and applications of high efficient energy conversion systems.

James F. Whidborne (M'95-SM'10) received the BA in engineering from Cambridge University and MSc and PhD in systems and control from University of Manchester Institute of Science and Technology (UMIST), UK.

From 1991-1994, he was a research associate with the Department of Engineering, University of Leicester. From 1994-2003, he was a lecturer, then senior lecturer with the Department of Mechanical Engineering, Kings College London. He is currently Head of the Dynamics Simulation and Control Group in the Department of Aerospace Engineering at Cranfield University, UK. His research interests are in the theory and application of advanced control, including multi-objective robust control design, fluid flow control, finite precision controller implementation problems, as well as flight control problems such as control and guidance of UAVs, controller reallocation and attitude control of VTOL aircraft.

He is a chartered engineer, a Member of the IET and a Senior Member of the IEEE.